Nonuniform Epicardial Activation and Repolarization Properties of in Vivo Canine Pulmonary Conus

Mary Jo Burgess, Bruce M. Steinhaus, Kenneth W. Spitzer, and Philip R. Ershler

The relation between nonuniform epicardial activation and ventricular repolarization properties was studied in 14 pentobarbital anesthetized dogs and with a computer model. In 11 dogs, isochrone maps of epicardial activation sequence were constructed from electrograms recorded from the pulmonary conus with 64 electrodes on an 8 × 8 grid with 2-mm electrode separation. The heart was paced from multiple sites on the periphery of the array. Uniformity of epicardial activation was estimated from activation times at test sites and their eight neighboring sites. Acceleration shortened and deceleration prolonged refractory periods. The locations of acceleration and deceleration sites of activation differed during drives from various sites, and differences in uniformity of activation during pairs of drives were correlated to differences in refractory periods ($\bar{r} = 0.76$, range 0.59–0.93). In three additional experiments, transmural activation sequence maps were constructed from electrograms recorded from needle-mounted electrodes placed upstream and downstream to epicardial activation delays. Activation proceeded from epicardium to endocardium upstream to the delays and from endocardium to epicardium downstream to the delays. A computer simulation of two-dimensional action potential propagation based on the Beeler-Reuter myocardial membrane model provided insights to the mechanism for the results of the animal experiments. The two-dimensional sheet modeled the transmural anisotropic histology of the canine pulmonary conus and corresponded to previous reports and histology of specimens from five experiments. Simulated activation patterns were similar to those found in the experimental animals. In addition, action potentials were electronically prolonged at sites of deceleration and shortened at sites of acceleration, results comparable to the animal experiments. Our findings demonstrate that the location of areas of nonuniform epicardial activation is dependent on drive site and that nonuniform activation electronically modulates repolarization properties. Therefore it seems likely that the site of origin of ectopic ventricular complexes, especially in ischemic myocardium where activation is nonuniform, could be an important determinant of whether ectopic activity initiates sustained tachyarrhythmias. (*Circulation Research* 1988;62:233–246)

Ventricular repolarization properties are largely but not entirely independent of ventricular activation sequence. Abildskov[1] found refractory periods were longer when activation was initiated at a test site than during fusion drives with collision of activation fronts near the test site. Toyoshima and Burgess[2] confirmed this finding and found that refractory periods decreased progressively as the distance between a test site and site of initiation of activation was increased. Subsequently, we found refractory periods were more dependent on activation sequence in ischemic than in nonischemic myocardium.[3] We hypothesized that the dependence of refractory periods on activation sequence was electronically mediated and that slow conduction in ischemic myocardium was the likely factor responsible for the greater dependence of refractory periods on activation sequence in ischemic than in normal myocardium. Results from a computer simulation of action potential propagation supported this hypothesis.[4,5] The present study was aimed at defining the relation between nonuniform activation and repolarization properties. The results indicate that the location of sites of acceleration and deceleration is dependent on activation sequence and that refractory periods have their greatest dependence on activation sequence at sites where activation accelerates or decelerates. (Preliminary results have been reported in abstract form.[6,7])

From the Nora Eccles Harrison Cardiovascular Research and Training Institute and the Department of Medicine, University of Utah, Salt Lake City, Utah.

Supported by National Institutes of Health-National Heart, Lung, and Blood Institute grant 5 RO1 HL 34288-02 and by awards from the Nora Eccles Treadwell Foundation and the Richard A. and Nora Eccles Harrison fund for Cardiovascular Research.

Address for correspondence and reprints: M.J. Burgess, M.D., Nora Eccles Harrison Cardiovascular Research and Training Institute, Building 100, University of Utah, Salt Lake City, UT 84112.

Received October 22, 1986; accepted July 31, 1987.

Materials and Methods

Animal Experiments

Experiments were done on 14 mongrel dogs anesthetized with bolus intravenous infusions of sodium pentobarbital (30 mg/kg). Additional bolus infusions of sodium pentobarbital (30–60 mg) were given as needed to maintain anesthesia. The chest was opened with a sternal splitting incision and the animal ventilated with room air via a pump respirator. The heart was suspended in a pericardial cradle, and the sinus node was crushed. The right atrial appendage was paced at 400-msec cycle lengths (S_1-S_1) delivered via a bipolar hook electrode. In 11 experiments, an electrode array, consisting of 64 unipolar silver electrodes mounted flush in a flat epoxy disk, was sutured on the epicardium in the region of the

pulmonary conus. The electrodes were 0.5 mm in diameter and arranged in an 8×8 grid with 2-mm spacing between center of columns and rows of electrodes. The columns of electrodes were positioned approximately parallel to the long axis of the superficial myocardial fibers, which was visually determined and corresponded to anatomic reports.[8] Histologic examination was done on specimens from five experiments to further document fiber orientation. The heart was paced simultaneously from the right atrium and single electrode sites on the periphery of the electrode array. A needle electrode placed subcutaneously in the right thorax served as the indifferent electrode for ventricular pacing. Atrial pacing stimuli were bipolar and ventricular stimuli were unipolar cathodal. Both the atrial and ventricular stimuli were of 2-msec duration, twice diastolic threshold constant current stimuli. In each experiment, the heart was paced from four to eight ventricular sites. Electrograms were simultaneously recorded from the electrode array at 1,000 samples/sec using a 64-channel multiplexer recording and data processing system. The characteristics of this system have been previously reported.[9] A Wilson central terminal was used as the reference electrode for recording. In several experiments, a reference electrogram was also calculated from the average signal of all epicardial sites, excluding the stimulation site. The calculated reference electrogram was subtracted from the electrograms recorded from each site. This procedure minimized the effects of distant events on the unipolar electrograms. Activation times at each site were chosen as the time, with respect to S_1, of the minimum derivative of the QRS in each electrogram referenced to the Wilson central terminal. Activation isochrone maps were displayed on a computer terminal, and during some experiments hard copies were obtained. On the basis of the isochrone maps, test sites in areas with marked differences in uniformity of activation during two activation sequences were chosen, e.g., a site where activation decelerated with one activation sequence and accelerated or was uniform with another activation sequence. All test sites were at least 5.7 mm away from the pacing sites. Our previous work[2] showed the effect of distance between test and drive site on refractory periods was minimal at distances greater than 4–6 mm. Refractory periods were measured with 2-msec-duration, twice-diastolic-threshold, constant-current cathodal stimuli delivered to the test site after every fourth S_1. The test stimuli (S_2) were delivered early in the cardiac cycle and delayed in 1-msec increments until a response occurred. This procedure minimized the effects of premature responses on refractory periods. The activation time at the test site was subtracted from the S_1-S_2 interval to determine the refractory period. Each drive was sustained for at least 3 minutes before the refractory period measurements were started. Five or more refractory period determinations were made during each drive, and 30–60 seconds were allowed to pass between measurements. The drive site was then changed, and five or more refractory periods were again measured at the same test site. The first site was again driven, and one or two more measurements were made to determine the stability of the preparation. If the refractory periods varied by more than 2 msec, the procedure was repeated. If stable measurements still could not be obtained, the data were discarded. The average refractory period for each drive was calculated. The same procedure was repeated to determine refractory periods at other test sites during other pairs of drives.

Given the epicardial location of the recording electrodes in these 11 experiments, the detailed three-dimensional path of activation was unknown. Hence, exact determination of conduction velocity was not possible. An estimate of uniformity of epicardial activation was calculated from activation time data and the geometric relation of the electrodes. Nonuniformity of activation was calculated as the sum of the differences in activation times between a test site and each of its eight neighbors divided by the interelectrode distances (Figure 1). Numbers calculated in this way will be referred to as the nonuniform activation index (NAI, msec/mm) and are equivalent to the second spatial derivative of activation time multiplied by the interelectrode distance. The theoretical basis for the relation between action potential configuration and the second spatial derivative of activation time is given in the "Appendix." A previously reported analytic development showed that conduction velocity is one of the five parameters that determine the electrotonic modulation of repolarization at sites of action potential collision.[5] The work presented in the "Appendix" extends these findings to spatial changes in conduction velocity and derives the NAI. The NAI provides a single quantitative index of uniformity of propagation in a discretely sampled area. Thus, the index reduces complex multidimensional activation patterns to one statistically useful parameter.

In the present study, the NAI was used to quantitate the relation between repolarization properties and the uniformity of activation. A positive NAI indicates slowing of epicardial activation or deceleration at the test site, and a negative NAI indicates acceleration at the test site. An NAI of 0 indicates uniform activation but does not indicate whether activation is fast or slow. The difference in NAI (ΔNAI) at a test site during a pair of drives and the difference in refractory period (ΔRP) at the same test site during the same pair of drives were calculated. Correlation coefficients between ΔRP and ΔNAI were calculated for individual experiments and for data pooled from all experiments.

In three additional experiments, transmural activation sequence was determined in regions upstream and downstream to sites of epicardial activation delays. A plaque with eight columns and four rows of electrodes was sutured to the pulmonary conus with the columns of electrodes placed approximately parallel to the long axis of the superficial epicardial fibers. Columns of electrodes were 2 mm apart, and rows of electrodes were 4 mm apart. There were also seven columns and three rows of holes centered between the columns and rows of electrodes in the plaque to permit transmural

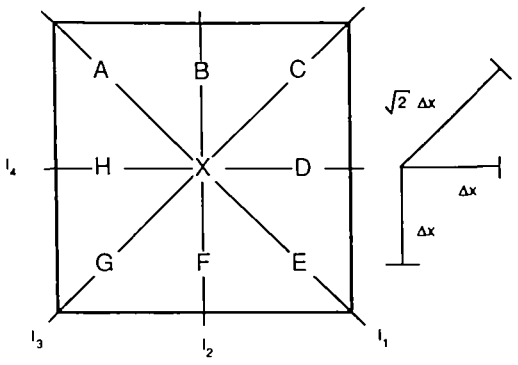

$$NAI_x = \sum_{i=1}^{4} \Delta I_i \frac{\partial^2 AT_x}{\partial I_i^2} \quad (1)$$

$$NAI_x = \frac{A-2X+E}{\sqrt{2}\,\Delta x} + \frac{B-2X+F}{\Delta x} + \frac{C-2X+G}{\sqrt{2}\,\Delta x} + \frac{D-2X+H}{\Delta x} \quad (2)$$

$$NAI_x = \frac{A-X}{\sqrt{2}\,\Delta x} + \frac{B-X}{\Delta x} + \frac{C-X}{\sqrt{2}\,\Delta x} + \frac{D-X}{\Delta x} + \frac{E-X}{\sqrt{2}\,\Delta x} + \frac{F-X}{\Delta x} + \frac{G-X}{\sqrt{2}\,\Delta x} + \frac{H-X}{\Delta x} \quad (3)$$

$$NAI_x = \frac{1}{\Delta x}\left[(B+D+F+H-4X) + \frac{1}{\sqrt{2}}(A+C+E+G-4X)\right] \quad (4)$$

FIGURE 1. *Nonuniform activation index (NAI) at electrode site X was calculated using activation time data from site X and its eight neighbors, sites A–H, whose locations are shown in* upper panel. *Epicardial activation can rarely be described as plane wave propagation with parallel isochrones. If this were the situation, spatial changes in conduction could be treated as a vector using measurements along two orthogonal axis. In this study, NAI was the sum of the second spatial derivative of time in four directions, I_1–I_4, times the electrode spacing (Equation 1). Second central difference formula was used in the estimation of the derivative terms with Δx as the electrode spacing (Equation 2). Equation 3 is derived to show that NAI is equal to the sum of the differences in activation times between the test site and each of its eight neighbors divided by the interelectrode distances. Reduced formula that was used in the automated computer routine is shown as Equation 4. See "Appendix" for theoretic basis for NAI.*

insertion of needle-mounted electrodes. Each needle-electrode array was 0.7 mm in diameter and had 12 unipolar 80-μm diameter electrodes spaced 1 mm apart. The needles were insulated except for the exposed surfaces of the electrodes. Epicardial activation maps were constructed during drives from single electrode sites at the periphery of the plaque electrode array. Areas of epicardial activation delays were identified, and five to seven needles were then inserted through the holes in the plaque to span the area of nonuniform activation. Electrograms were recorded simultaneously from the 60–84 needle-mounted electrodes and the 32 electrodes on the epicardial plaque using a 192-lead multiplexed data acquisition and processing system.[10]

Histology

At the conclusion of three experiments in which transmural activation sequence was studied and two experiments in which refractory periods were measured, the pulmonary conus was excised and fixed in 10% buffered formalin. Transmural sections were cut perpendicular to the epicardium at 2-mm intervals to correspond to electrode spacing. The cuts were made parallel to the superficial epicardial fibers in two specimens and perpendicular to them in three specimens. The specimens were routinely processed, paraffin embedded, stained with H and E and Masson's trichrome stain, and examined with a light microscope.

Computer Simulations

Computer simulations of two-dimensional action potential propagation were used to gain insights to the mechanism for the changes in location of epicardial activation delays during different activation sequences observed in the animal experiments. Transmural ventricular propagation was simulated by assuming the two-dimensional sheet represented a continuous plane oriented perpendicular to the epicardial and endocardial surfaces of the ventricular wall. The sheet was partitioned into a thick epicardial and a thin endocardial layer by modeling the epicardial layer using transverse cell-to-cell coupling resistance values in both directions and modeling the endocardial layer using transverse resistances in the transmural direction and longitudinal resistances in the other direction. This arrangement models the fiber orientation previously reported to exist in the region of the canine pulmonary conus[8] and confirmed by the histology of specimens from our experiments. The two-dimensional model used in this study differs from the two electrically interactive cables reported by Joyner et al[11] in that our model allows continuous transmural propagation. The two-dimensional model consists of electrically connected membrane segments defined by the Beeler-Reuter membrane model[12] with the reversal potential for the slow inward current fixed at 70 mV. Identical intrinsic membrane properties were assigned to all segments. The differential equation relating the membrane segments is an extension of the cable equation to two dimensions:

$$I_m = \frac{1}{Sv}\cdot\left[\frac{1}{Ri_x}\cdot\frac{\partial^2 Vm}{\partial x^2} + \frac{1}{Ri_y}\cdot\frac{\partial^2 Vm}{\partial y^2}\right] = C_m\cdot\frac{\partial Vm}{\partial t} + I_i \quad (1)$$

where I_m is the membrane current (μA/cm²); Sv is the surface to volume ratio of the cells (cm^{-1}); Ri_x and Ri_y are the specific cell-to-cell resistivities in the x axis and y axis directions (kΩcm); Vm is the transmembrane voltage (mV); C_m is the specific membrane capacitance (μF/cm²), and I_i is the total ionic current (μA/cm²). The sheet was terminated in open circuits on all four sides. The cellular cytoplasmic and junctional resistances were combined to form the equivalent segment cell-to-cell resistivity (Ri).

Two types of anisotropy in the epicardial layer were

modeled, uniform and nonuniform.[13] The uniform model had cell-to-cell resistances that were uniformly higher in the transverse direction than in the longitudinal direction. The increased resistivity in the transverse direction modeled the overall resistive effects of cellular packing with reduced occurrence of intercalated disks in the transverse direction compared with the longitudinal direction.[14] The nonuniform anisotropy model, like the uniform model, had cell-to-cell resistances that were higher in the transverse than the longitudinal direction. However, in this case, the magnitudes of the higher transverse junctional resistances were nonuniformly distributed. This nonuniform distribution of junctional resistances was assumed to represent reduced electrical coupling of transverse cellular connections caused by connective tissue and/or reduced occurrence of gap junctions. In the experimental animals, areas of epicardial activation delays as great as 20 msec were often observed across a 2-mm distance. The activation delays were generally oriented parallel to the long axis of the superficial epicardial fibers. In the transmural maps, activation delays of similar magnitude were found underlying the epicardial activation delays and were perpendicular to the epicardium. Therefore, we modeled the electrical uncoupling of cell connections as affecting only transverse connections in the epicardial layer, which were oriented perpendicular to the epicardial surface (see Figure 6, lower panel). It was assumed that only junctional resistances of cell-to-cell connections were affected and that extracellular resistance was unaltered. Resistivity of cell-to-cell connections in these areas of uncoupling was not assigned an infinite value because it was assumed that over the length of the numerical segment, several low-resistance junctional pathways still existed. Areas of electrical uncoupling were randomly distributed. Although recent studies report a possible directional difference in membrane capacitance,[15] this feature was not implemented. In addition, previous analytical and simulation studies have shown that collision effects on action potential repolarization are independent of inhomogeneity in action potential duration[5]; therefore, we did not assign an epicardial-to-endocardial gradient in action potential duration but did assign uniform properties to all membrane segments. Thus, inhomogeneity in action potential durations was solely the result of electrotonic interactions.

The equations describing the complete model were numerically solved by finite difference techniques using the Crank and Nicholson implicit method[16] and an alternating direction scheme[17,18] similar to previous reports.[19] A more detailed description of the numerical solution methods has been previously published.[20] Typically, each action potential was described by about 500 points, approximately 200 of which were in the upstroke. Activation time was chosen as the elapsed time from the start of the simulation to the upstroke, calculated at Vm = −80 mV. Action potential duration was computed at Vm = −80 mV. Each numerical integration segment was a parallelepiped with edges of length Δx, Δy, and Δz (cm). Extracellular potential waveforms at selected positions were calculated assuming a homogeneous volume conductor surrounded the myocardial model. This assumption does not model the effects of either restricted extracellular space or extracellular anisotropy. While this assumption is only valid as a first-order approximation, the simulated electrograms were similar to those recorded in the animal experiments. The following equation[21,22] was used:

$$EG_x(t) = \frac{Re}{4\pi} \sum_{i=1}^{M} \sum_{j=1}^{N} \frac{I_{m_{i,j}}(t)(\Delta x \Delta y \Delta z)Sv}{d_{i,j}} \quad (2)$$

where $EG_x(t)$ is the electrogram potential at position x and time t (μV), Re is the extracellular resistivity (Ωcm), M and N are the total number of numerical segments in the x and y directions, $d_{i,j}$ is the distance from electrode position x to numerical segment (i,j) (cm), $I_{m_{i,j}}(t)$ is the membrane current (μA/cm^2), Sv is the surface-to-volume ratio of the cell (cm^{-1}), and Δx, Δy, and Δz are the spatial step sizes in the x, y, and z directions (cm). The electrograms were computed for an electrode position at a distance of 225 μm above the epicardial edge of the sheet surface.

The standard parameter settings were Δx (spatial step size x direction) = 0.45 mm, Δy (spatial step size y direction) = 0.45 mm, Δz (spatial step size z direction) = 0.02 mm, surface-to-volume ratio = 5,000/cm, sheet size = 1.4 cm × 0.68 cm × 0.002 cm, total number of segments = 512 (32 × 16 grid), C_m = 1.0 μF/cm^2, cycle length = 800 msec, Ri (longitudinal axis) = 250 Ωcm, Ri (transverse axis) = 900 Ωcm, Ri (areas of increased cell-to-cell resistance, nonuniform model) = 9,000 Ωcm, and Re = 100 Ωcm. Propagation was initiated by a square pulse of intracellular depolarizing current, twice diastolic threshold and 2 msec long. Stimuli were applied to five contiguous cells, unless otherwise indicated. To ensure steady-state conditions, each run consisted of pacing the cable twice with data recorded on the last beat. Programs were written in Fortran using double precision variables. An 800-msec simulation required about 3 hours of CPU time using either a Digital Equipment Corporation VAX 11/750 or MicroVAX-II computer.

Results

Animal Experiments

Isochrone maps of two activation sequences from a dog, one sequence initiated at the top near the center of the array and one initiated at the bottom near the center of the array, are shown in Figure 2. Four sites at which refractory periods were measured during each drive are indicated by the numbers on the isochrone maps, and refractory periods and NAIs measured at those sites during each drive are indicated beneath the isochrone maps. Conduction velocity, calculated as distance between electrodes divided by the differences in their activation times, was faster in the direction parallel to the long axis of myocardial fibers than in the

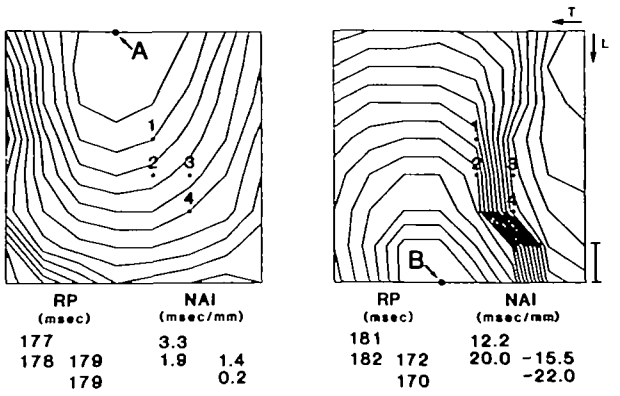

FIGURE 2. *Epicardial isochrone maps of activation in region of pulmonary conus during drive A,* left panel, *and drive B,* right panel, *are shown. Refractory periods (RP) and nonuniform activation index (NAI) during each drive are listed below maps and arranged to correspond to four test sites (1–4) indicated on maps. During drive A, NAIs were 3.3 msec/mm or less indicating little acceleration or deceleration at test sites, and RPs ranged from 177 to 179 msec. During drive B, NAIs at sites 1 and 2 were 12.2 and 20.0 msec/mm, respectively, indicating deceleration, and RPs were longer than they were during drive A. NAIs at sites 3 and 4 were −15.5 and −22.0 msec/mm during drive B, indicating acceleration, and RPs were shorter than they were during drive A. T and L indicate transverse and longitudinal fiber orientation. Isochrones are drawn at 2-msec increments, and the spatial calibration bar is 2 mm.*

direction perpendicular to them. For the data shown in Panel A, conduction velocity averaged 0.58 m/sec in the fast longitudinal direction and 0.39 m/sec in the slow transverse direction, values comparable to previous reports.[23–27] During drive A, activation of the four test sites was relatively rapid and uniform. During drive B, however, there was an area of epicardial activation delay to the right of the vertical midline of the array. The NAIs at sites 1 and 2 were 12.2 and 20.0 msec/mm, indicating deceleration. Refractory periods at these two sites were 181 and 182 msec during drive B compared with 177 and 178 msec during drive A. The NAIs at sites 3 and 4 were −15.5 and −22.0 msec/mm during drive B, indicating acceleration. Refractory periods at sites 3 and 4 were 172 and 170 msec during drive B compared with 179 msec at both sites during drive A. The differences in NAI (ΔNAI) at sites 1 and 2 between drive B and A were 8.9 and 18.1 msec/mm, respectively, indicating relative deceleration at these sites during drive B in comparison with drive A. This was associated with refractory periods 4 msec longer at both sites 1 and 2 during drive B than during drive A. ΔNAIs at sites 3 and 4 were −16.9 and −22.2 msec/mm, respectively, indicating relative acceleration at these sites during drive B as compared to drive A. This was associated with refractory periods 7 and 9 msec shorter at sites 3 and 4 during drive B than during drive A. These findings demonstrate that deceleration was associated with prolongation of refractory periods and acceleration was associated with shortening of refractory periods.

The magnitude of nonuniform activation varied in different animals. Over all 11 experiments, the greatest deviation of NAI from zero at any test site during any drive averaged 22.1 msec/mm (range 6.6–35.6 msec/mm). The maximum deviation of NAI from zero at any test site during any drive was less than 10 msec/mm in only one animal. To assist in relating these NAI values to the magnitude of activation delays, refer to Figure 2. Correlation coefficients between ΔRP and ΔNAI were calculated for each experiment and ranged from 0.59 to 0.93. The correlation coefficient between ΔRP and ΔNAI for data pooled from all 11 experiments was 0.76 ($n = 115$).

Examples of the spatial changes in epicardial activation delays during different drives are illustrated in the maps in Figure 3. Shown in the upper six panels are activation sequence maps from one dog during pacing of six epicardial electrode sites. Activation delays were generally oriented parallel to longitudinal fiber axis, but during different drives, the delays occurred at almost all locations of the sampled area. The lower panel of Figure 3 shows maps from another dog and demonstrates the differing effects of epicardial and endocardial stimulation on the presence of epicardial activation delays. Propagation from epicardial drive A (left panel) resulted in activation delays in the center of the electrode array. In contrast, drive via a unipolar plunge electrode located on the endocardial surface approximately below site A (right panel) resulted in no activation delay.

In these experiments, changes in uniformity of epicardial activation were solely the result of changes in pacing site. No interventions were used that would be expected to alter membrane properties. It, therefore, seems likely that the observed changes were due to anatomic features of the right ventricular myocardium and the three-dimensional spread of activation. This hypothesis is supported by the epicardial and transmural activation sequence maps and selected electrogram shown in Figure 4. The maps were constructed from data recorded from 32 epicardial surface electrodes and seven needle-mounted multielectrode arrays. Maps from two dogs are shown. The location of the plane of the transmural maps is indicated in the diagram at the top of the figure. The stars on the epicardial maps indicate the sites of insertion of the needle-mounted electrodes. Maps constructed from epicardial surface electrograms recorded before and after insertion of the needle electrode arrays did not differ from each other. In the maps shown on the left of the figure, the heart was paced at epicardial site A. On the epicardial surface, activation was faster along the long axis of fibers than across the transverse fiber axis, but in each direction, activation was relatively uniform. This pattern of activation is consistent with uniform anisotropy. On the transmural plane, activation initially spread radially from the epicardium near drive site A, the upper right portion of the map. Later, activation fronts were approximately perpendicular to the epicardium. Activation then proceeded faster on the endocardium than on the epicardium, a finding con-

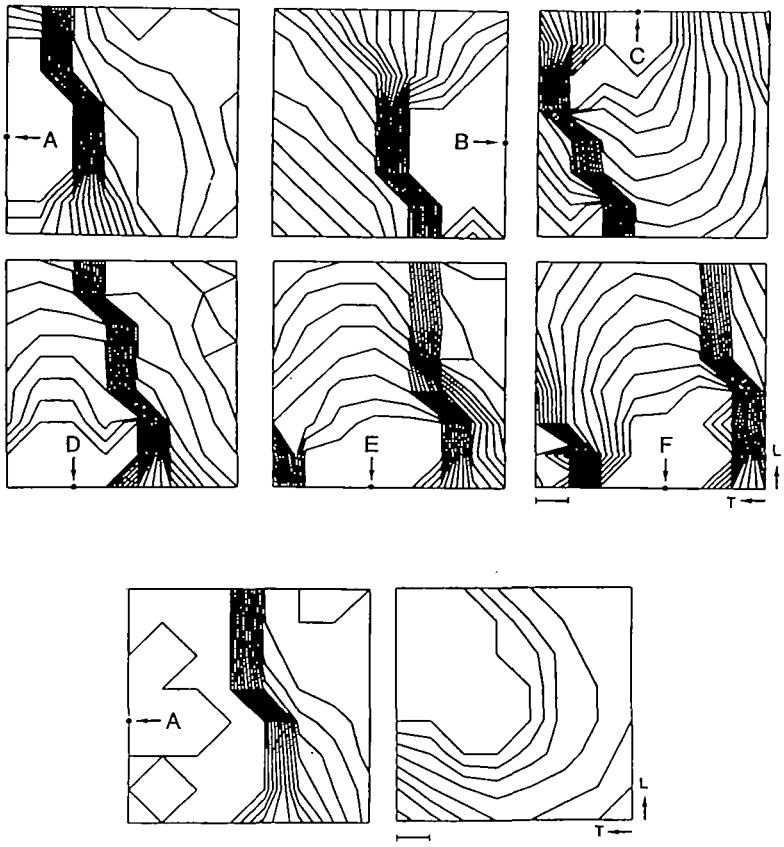

FIGURE 3. *Effect of stimulus site on location of activation delays in pulmonary conus. Isochrone maps in upper portion of figure were recorded from a dog during drive of six sites, A–F. Areas of slow activation had different locations during different drives. Two isochrone maps at the bottom of the figure are from another dog and were recorded during drive of epicardial site A,* left panel, *and an endocardial site located transmurally below epicardial site A,* right panel. *Activation delays were less marked during endocardial drive than during epicardial drive. Isochrones are drawn at 2-msec increments, the spatial calibration is 2 mm, and T and L indicate transverse and longitudinal fiber orientation.*

sistent with longitudinal orientation of epicardial fibers. Then activation fronts slowly rotated, and activation spread obliquely from endocardium to epicardium. Maps from another dog are shown on the right side of the figure. The heart was paced from site B. As in the map on the left, epicardial activation was faster along the long axis of the fibers than transverse to them. However, an area of activation delay that cannot be explained on the basis of uniform fiber orientation alone can be seen near the center of the epicardial map. An area of activation delay, underlying the epicardial activation delay, can also be seen on the transmural map. Upstream to the delay, activation proceeded obliquely from epicardium to endocardium. Downstream to the delay, the activation fronts rotated abruptly, and activation proceeded from endocardium to epicardium. The waveforms recorded at sites 1 and 2 are shown at the bottom of the maps. Electrograms from sites where activation fronts proceeded from the epicardium to the endocardium (site 2, left panel, and site 1, right panel) had predominantly negative QRS complexes and positive T waves. In contrast, predominantly positive QRS complexes and negative T waves were recorded from sites where activation proceeded from the endocardium to the epicardium (site 1, left panel, and site 2, right panel).

Histology

In all specimens examined, fibers were uniformly distributed in the endocardial and epicardial layers. The fibers within a layer were parallel to each other, and the two layers of fibers were orthogonally orientated. A section of the pulmonary conus of one dog is shown in Figure 5. The section was cut perpendicular to the epicardial and endocardial surfaces and perpendicular to the long axis of epicardial surface fibers. Therefore, the fibers in the epicardial layer are seen on end, and this layer is approximately one half the thickness of the ventricular wall. Although slight differences in fiber orientation might not be detected on this section, the arrangement of fibers within the outer and inner layers of the ventricular wall seemed uniform. Longitudinally oriented fibers were encountered in the inner half of the ventricular wall, and rotation of fibers between the outer and inner layers occurred abruptly, in accord with previous work.[8] The ratio of the thickness of the layers of orthogonally oriented fibers varied between animals. In the example shown, the endocardial layer was thicker than previously reported.[8] However, in other animals, the proportions of epicardial to endocardial layers correspond to the previous report. An orthogonal relation between epicardial and endocardial layers and abrupt rotation of fibers between layers was observed in all five specimens. The dark areas in the photomicrographs are collagenous material that stained blue with trichrome. Collagen was distributed throughout the epicardial layer.

Computer Simulations

Additional evidence for the mechanism of epicardial activation delays was obtained in a computer simulation of action potential propagation. Transmural propagation was simulated in a two-dimensional sheet oriented perpendicular to the epicardial and endocar-

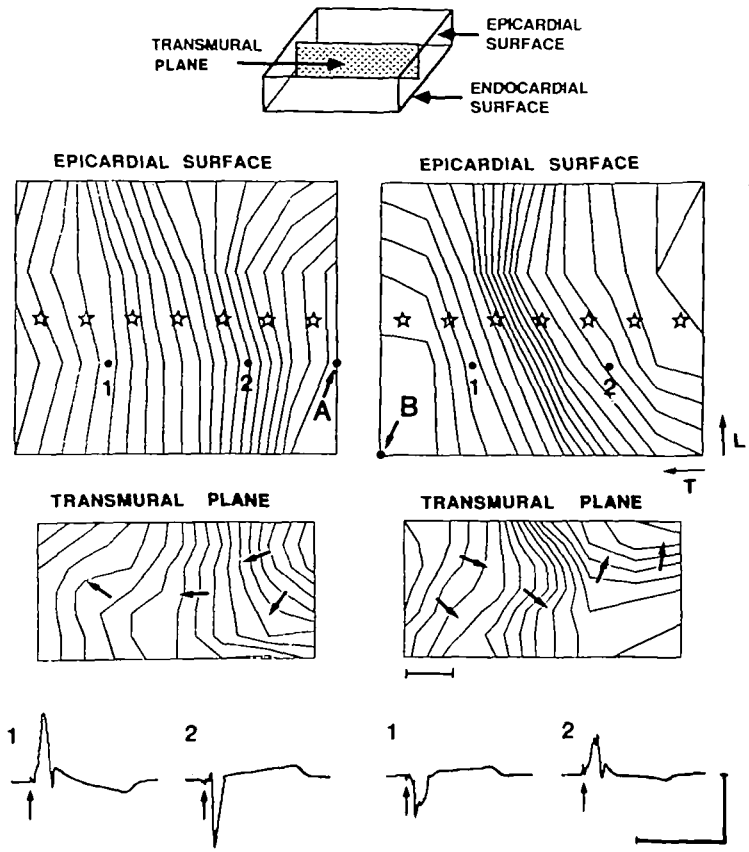

FIGURE 4. *Epicardial and transmural activation sequence maps constructed from simultaneously recorded electrograms from pulmonary conus of two dogs. A diagrammatic representation of a block of pulmonary conus is shown at the top of the figure. Transmural maps are of plane indicated by stippled area in diagram and were constructed from data recorded from seven needle-electrode arrays inserted at sites indicated by stars on epicardial activation maps. Arrows indicate direction of activation. In the map shown on the left, activation is relatively uniform on the epicardial surface. On the transmural plane, activation spread radially from epicardium to endocardium; then the wavefronts gradually rotated and spread obliquely from endocardium to epicardium. There were no areas of activation delays. In the map shown on the right, an area of activation delay can be seen in both epicardial and transmural maps. On the transmural maps, activation fronts rotate sharply downstream to the delay and are approximately parallel to the epicardial surface. Electrograms from epicardial sites 1 and 2 are shown below maps. Reference signal for the electrograms was the average signal of all epicardial sites, excluding the stimulus site. Isochrones are drawn at 2-msec increments, and calibration bars are 200 msec and 20 mV. Spatial calibration bar is 2 mm.*

dial surfaces. Both uniform anisotropy and nonuniform anisotropy were modeled. Nonuniform anisotropy was modeled by assigning higher cell-to-cell resistances to a random distribution of discontinuous areas oriented perpendicular to the epicardial surface. Figure 6 shows the transmural activation sequence following stimulation at the indicated epicardial site of the uniform anisotropy model. The transmural spread of excitation was relatively uniform across the ventricular wall, and there were no marked activation delays. Near the drive site, wavefronts spread radially from epicardium to endocardium. Further from the drive site, wavefronts were approximately perpendicular to the epicardial surface with the most rapid conduction velocity occurring along longitudinally oriented fibers on the endocardial layer. At the right side of the transmural plane, wavefronts slowly rotated upward toward the epicardial surface. The surface electrograms (EG) membrane current waveforms (I_m) and epicardial surface action potential durations (APD) were all consistent with propagation in a uniform anisotropic medium. This model was unable to account for the nonuniform activation and repolarization changes observed in the animal experiments. The bottom panel shows the activation sequence in the nonuniform anisotropy model after stimulation at the indicated epicardial site. An area of marked epicardial and transmural activation delay can be seen in the left center of the maps. Downstream to the delay, activation rapidly proceeded along the endocardial layer, and the activation fronts rotated sharply along the epicardial surface. Propagation then proceeded nearly parallel to the areas of increased cell-to-cell resistance. With this orientation of wavefronts, the higher cell-to-cell resistances were nearly perpendicular to the activation fronts, and activation was relatively uniform. As shown in the plot of epicardial surface APD, duration increased at sites upstream from the delay and decreased downstream from the delay.

When the endocardial layer was removed from the nonuniform anisotropy model, initial activation near the site of epicardial stimulation was very similar to that in the model with the endocardial surface. However, at sites greater than 4 mm from the stimulus site, activation fronts did not bend upwards toward the epicardium but were oriented perpendicular to the epicardial surface, and epicardial conduction velocity was very slow (0.144 m/sec). In addition, action potential durations were highly disparate across the whole epicardial surface. Thus, the presence of the endocardial layer markedly affected the homogeneity of both epicardial activation and recovery patterns and was necessary to account for the experimental results.

A mechanism for the APD and activation pattern changes shown in Figure 6 is suggested from the membrane current (I_m). I_m waveforms from two sites adjacent to the epicardial activation delay are shown. In both the uniform and nonuniform models, I_m at site 1 (I_{m_1}) has a larger negative than positive component during depolarization, indicating electrotonic loading by underlying sites. During repolarization, I_{m_1} in both models is entirely positive, indicating electrotonic

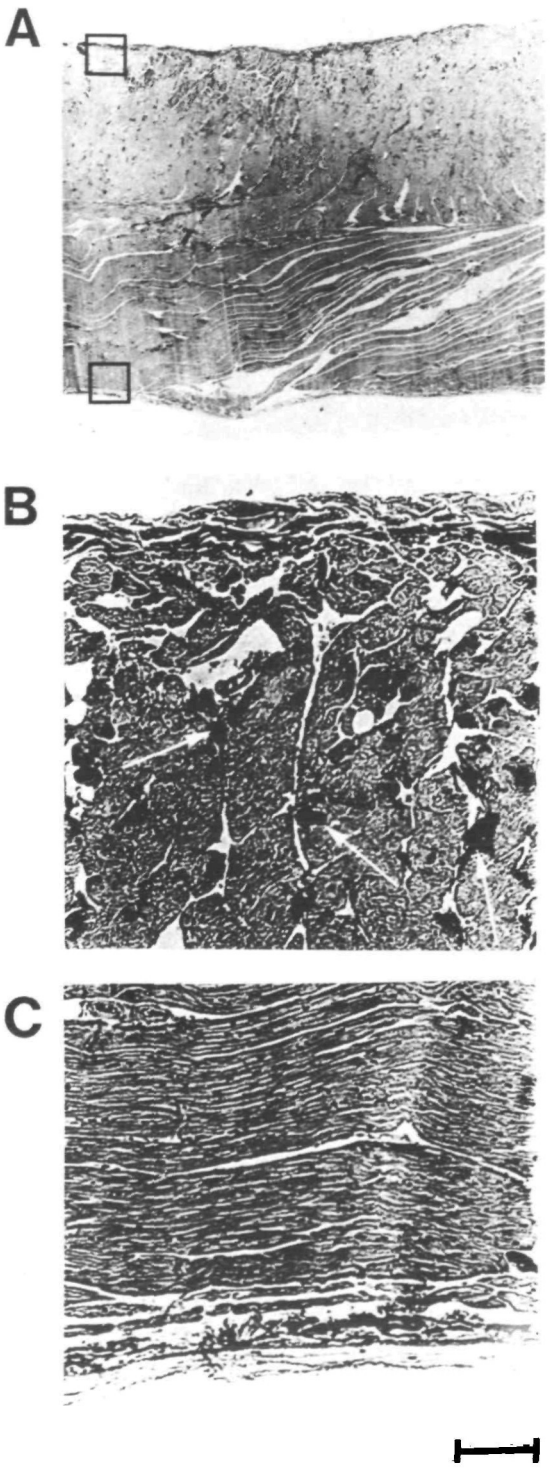

FIGURE 5. *Transmural trichrome stained section of pulmonary conus is shown at low magnification in* Panel A. *Specimen was cut perpendicular to longitudinal axis of superficial epicardial fibers. Clear areas in Panel A are artifacts that occurred during preparation of slide. Squares in Panel A designate magnified portions of epicardium* (Panel B) *and endocardium* (Panel C). *White arrows in Panel B indicate some of the collagenous material that stained dark blue with trichrome. Spatial calibration bar is 1.12 mm (Panel A) and 0.1 mm (Panels B and C).*

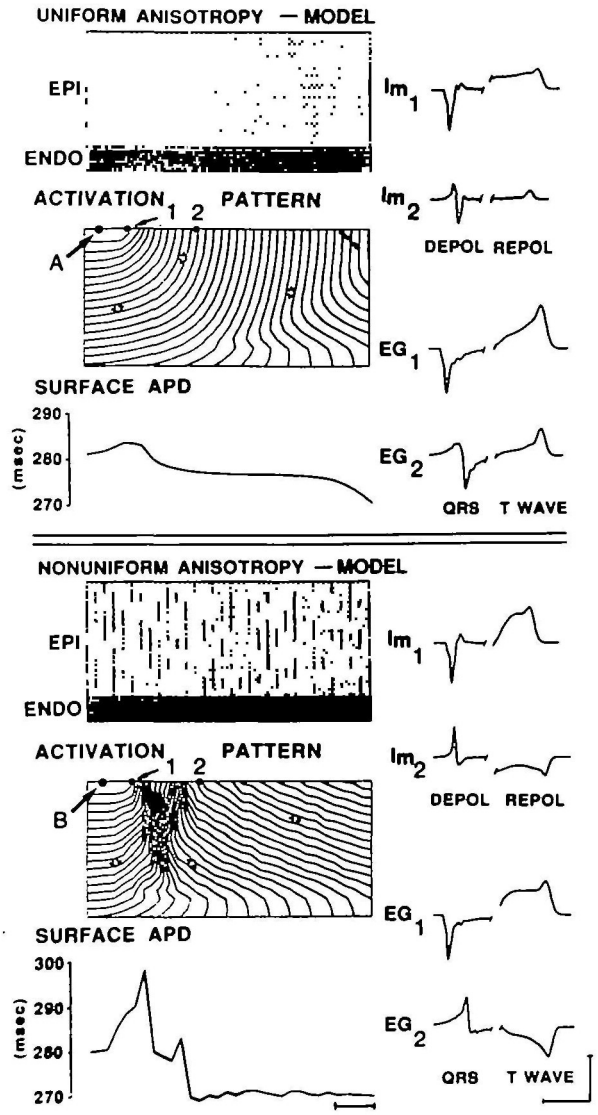

FIGURE 6. *Simulated transmural propagation in model of uniform and nonuniform anisotropy. Fibers in epicardial (epi) and endocardial (endo) layers are diagrammed in the* upper panel. *Locations of areas of increased cell-to-cell resistance in epicardial layer of nonuniform anisotropy model are indicated by vertical lines. Following epicardial stimulation, activation dove to endocardium. Activation then rapidly spread along endocardium and back to epicardium. In nonuniform anisotropy model, areas of increased cell-to-cell resistance downstream to delay had less effect on spreading activation than areas of increased cell-to-cell resistance near the stimulation site because activation fronts were nearly parallel to these areas. Membrane current waveforms (I_m) and electrograms (EGs) from sites 1 and 2 are shown. Waveform horizontal calibration bars: 5 msec (I_m depolarization), 100 msec (I_m repolarization and EG T wave), 20 msec (EG QRS complex). Waveform vertical calibration bars: 100 μA/cm² (I_m depolarization), 0.3 μA/cm² (I_m repolarization), 2.2 mV (EG QRS complex), and 0.044 mV (EG T wave), spatial calibration 2 mm. Number of cells = 32 × 16. Rows 1–13 represent epicardial layer (Ri in both directions = 900 Ωcm). Rows 14–16 represent endocardial layer (Ri_x = 250 Ωcm, and Ri_y = 900 Ωcm). Isochrones are drawn at 2-msec increments.*

charging due to the wavefront moving toward the endocardium. This charging is greatly increased in the nonuniform anisotropy model due to the close proximity of site 1 to the activation delay. At site 2 in the uniform model, I_m during depolarization (I_{m_2}, depol) is biphasic with nearly equal positive and negative components, consistent with uniform propagation.[4,5] In contrast, I_{m_2} (depol) in the nonuniform anisotropy model is almost entirely positive because the wavefront collided with the epicardial surface. Although uniform intrinsic membrane properties were assigned in these simulations, electrotonic charging during repolarization in the nonuniform model resulted in an action potential duration of 288 msec at site 1, while at site 2, electrotonic loading during repolarization resulted in an action potential duration of 269 msec, a difference of 19 msec. The EGs closely parallel the I_m waveforms. In the nonuniform model, they reflect loading at site 1 and charging at site 2 during depolarization and charging at site 1 and loading at site 2 during repolarization. The waveshape of EG_1, upstream from the activation delay in the nonuniform anisotropy model, was similar to the tissue electrogram at the site upstream to the activation delay shown in Figure 4. Both simulated and recorded EGs have a negative QRS complex and a positive T wave. Downstream from the delay, the simulated and recorded EGs have a positive QRS complex and a negative T wave. The changes in EG shape reflect the underlying changes in electrotonic current and are not due to boundary effects of the limited simulated model dimensions per se.

Assuming the nonuniform anisotropy model in Figure 6 represents the key features necessary to account for our experimental results, further simulations were performed to examine the influence of stimulation site on activation pattern. The results closely paralleled the dependence of locations of activation delays on drive site seen in the animal experiments (Figure 3). As in the animal experiments, epicardial activation delays occurred near the site of epicardial stimulation, and there were no marked epicardial activation delays in response to endocardial stimulation. In addition, the epicardial distribution of action potential durations was highly dependent on the stimulus location. When the model was stimulated from the endocardial surface, a very homogeneous epicardial surface action potential duration distribution resulted with only a 1.03-msec difference between the site with the maximum and minimum durations (271.12 -270.09 msec).

Discussion

Results from both animal experiments and computer simulations previously reported from our laboratory suggested that conduction velocity is a major factor in the dependence of repolarization properties on activation sequence. The studies reported here were designed to establish the relation of nonuniform activation to repolarization properties. To accomplish this, differences in uniformity of epicardial activation during pairs of drives were related to differences in refractory periods during the same pairs of drives. Nonuniformity of activation was calculated from activation times at the test site, and its eight neighboring sites and the distances between the test site and its neighbors. The NAI provided an estimate of acceleration or deceleration at the test site. The theoretic basis for this index is presented in the "Appendix." A negative NAI indicated that epicardial activation approached the test site slower than it moved away from it (acceleration), and a positive NAI indicated that epicardial activation approached the test site faster than it moved away from it (deceleration). The NAI would be zero if differences in activation times among neighboring sites were uniform, regardless of whether conduction velocity was rapid or slow. Therefore, the index provides an estimate of acceleration or deceleration of activation rather than conduction velocity.

Conduction velocity is known to be dependent on myocardial fiber orientation,[23-27] and the pulmonary conus preparations displayed faster activation longitudinal to fiber axis than transverse to fiber axis. However, during some activation sequences, regions of marked deceleration of epicardial activation were observed that did not seem to be related to fiber orientation alone. Nonuniform activation (NAI>10 msec/mm) was detected at one or more test sites during at least one activation sequence in 10 of 11 animals studied. Tsuboi et al reported nonuniform activation patterns in 15 of 40 in vitro canine pulmonary conus preparations.[28] They discarded such preparations from their study because they attributed the delays to tissue injury resulting from dissection. We found a greater incidence of nonuniform activation than Tsuboi et al, probably, because we specifically searched for areas of activation delays during pacing from multiple sites. While the experiments do not reveal the exact physiological basis of the activation delays, several possibilities exist. These include tissue injury, regional differences in membrane properties, and areas of increased cell-to-cell resistance.

We had no evidence that tissue injury was responsible for the activation delays. The electrodes on the plaque array were flush to the surface of an epoxy disk and did not penetrate the epicardial surface. The entire array was attached to the pulmonary conus via sutures placed at the periphery of the disk, the sutures were at least 4 mm from the closest electrode, and there was no ST segment displacement in the electrograms to indicate tissue injury.

Although regional differences in membrane properties, such as a localized decrease in excitatory sodium current, would slow propagation, the conduction velocity in such an area would not be dependent on activation sequence. Since the myocardium was well perfused in our experiments and because regions of activation delays had different locations during various drives, spatial differences in membrane properties were unlikely responsible for the changes.

We propose that the regions of abrupt slowing in epicardial activation observed with some activation sequences but not with others resulted from activation

proceeding through areas of increased cell-to-cell resistance. Increased cell-to-cell resistance may result from a reduction in numbers of gap junctions. This, in turn, could be due to either a regional transition in fiber orientation[29] or extracellularly distributed collagen.[13] Our histologic studies revealed no evidence of marked changes in epicardial fiber orientation that could account for the observed epicardial conduction delays. The studies suggested collagen distributed in the epicardial layer of the ventricle was a possible source of increased cell-to-cell resistance. We did not characterize the fine three-dimensional structure of the collagen (i.e., rods versus septa[13]) but did document that it was widely distributed in the outer layers of the pulmonary conus specimens examined. Spach and Dolber reported age-related differences in transverse electrical cell-to-cell coupling in human atria.[30] Similar age-related changes in ventricular cell-to-cell coupling could account for the differences in magnitude of activation delays observed among animals in the present study. However, since the ages of the animals were unknown, this possibility cannot be addressed. With our 2-mm electrode spacing, one or multiple areas of increased resistance located between the electrodes would have identical manifestations in the activation maps. In the experiment shown in Figure 3, activation delays were present over almost the entire sampled area when all activation sequences are considered. This suggests that areas of increased resistance were diffusely distributed and is compatible with electrical uncoupling of transverse myocardial fibers.

Regardless of the cellular basis of the increased cell-to-cell resistance, the three-dimensional aspects of the pulmonary conus played a key role in creating the activation patterns and accompanying repolarization changes. Unlike the case for a one-dimensional cable with a region of increased cell-to-cell resistance, the three-dimensional properties of the intact pulmonary conus provided an additional conductive pathway, allowing the epicardially initiated activation to spread transmurally towards the endocardium. On encountering longitudinally oriented cells in the endocardial layer, activation spread rapidly, and the activation fronts rotated. The reorientation of activation fronts resulted in propagation from endocardium to epicardium and collision at the epicardial surface. This initiation of activation on the epicardium and subsequent collision of activation at the epicardium produced, in effect, conditions similar to those during propagation in a one-dimensional cable terminated in open circuits. Mathematical models and tissue experiments of one-dimensional action potential propagation in heart muscle and other excitable membranes have shown that the sites of initiation and termination (equivalent to collision) of action potential propagation produce changes in conduction velocity and action potential configuration.[4,5,31-37] Electrical loading during the upstroke occurs at the site of initiation of action potential propagation. This results in decreased conduction velocity, increased action potential duration, decreased positive phase and increased negative phase of the extracellular potential during the upstroke, and decreased action potential amplitude and maximum upstroke velocity. Once the action potential propagates some distance, the configuration stabilizes. In contrast, at the site of action potential termination, opposite changes in conduction velocity, action potential configuration, and extracellular potential occur.

Support for the hypothesis that electrical uncoupling is the basis for the activation delays is shown in the activation sequence maps and electrograms in Figure 4, in the histology of the pulmonary conus in Figure 5, and in the simulations using the nonuniform anisotropy model in Figure 6. There was good agreement between the computer simulations and animal experiments. First, location of areas of activation delay differed when drive site was moved. Second, there were predominantly negative deflections in the QRS of EGs from sites just upstream to the areas of activation delay and positive deflections from EGs from sites just downstream. Opposite deflections occurred in the T waves of EGs upstream and downstream to the delays. Third, sites just upstream to areas of activation delay had increased refractory periods (animal experiments) and action potential duration (computer simulations), while opposite effects occurred just downstream to the delay. Fourth, areas of epicardial activation delays were less marked during endocardial than during epicardial pacing. Although refractory periods were not determined in the computer simulation, previous simulation studies from our laboratory have shown that refractory periods from simulated normal myocardium are altered in a similar manner to action potential duration.[5]

While other models may explain our results, the present simulations accounted for the main features of the experimental findings. Several other models incorporating barriers in various locations, including barriers placed parallel to the epicardium and endocardium, did not account for the experimental findings. In spite of the good agreement between our simulations and tissue experiments, there are limitations to the model. Although the Beeler-Reuter model does not include a quantitative description of all ionic currents responsible for mammalian myocardial action potential formation, it is a reasonable approximation of net ionic current. In addition, the simulated collision-induced changes in action potential duration are very similar to those observed in mammalian ventricular muscle.[5] Modeling transmural propagation in the pulmonary conus as a two-dimensional plane was a simplification given the complex three-dimensional properties of the area. Our rationale for this approach is based on the following. Consider the hypothetical case of a three-dimensional block of tissue composed of identical transmural planes that are identically coupled to each other electrically and activated simultaneously along a line that intersects each transmural plane at identical sites. In this situation, activation of the block will occur as a planar wave with no electrotonic interactions between planes. Since each plane will have identical propagation and repolariza-

tion patterns, one plane is sufficient to fully characterize the block. While this is clearly an idealized situation, epicardial activation in the pulmonary conus usually proceeded along spatially broad fronts, maintaining parallel orientations of activation over several millimeters. This was especially apparent at sites of activation delay (Figures 2, 3, and 4). In addition, serial histological sections revealed a fairly uniform geometry of the outer and inner layers of the pulmonary conus. Thus, it seemed appropriate as a first-order approximation to model transmural propagation as a two-dimensional plane, recognizing it omits current pathways in the third dimension. Another limitation was the assumption of negligible extracellular resistance in comparison to cell-to-cell resistance. Although this is a valid assumption for superfused isolated one- and two-dimensional tissue preparations, it was an approximation for the situation modeled in this study. Large numerical spatial step sizes such as those used in the simulations reported here introduce changes in the computed action potential configuration when compared with simulations using much smaller step increments.[38] This is due to the finite difference solution technique that was used to solve Equation 1 and assumes isopotential values across each numerical segment and lumped resistance values between segments. The effects of this discretization error on the electrotonic effects of action potential collision have been reported in a previous study.[5] In brief, large spatial step sizes decrease conduction velocity, which increases the electrotonic currents during action potential propagation. This increases the action potential duration changes at sites of activation initiation and collision. Because of its size, the numerical segment used in this study models the characteristics of multiple physiological cells. Previous simulations have used multiple numerical segments for each physiological cell and have included a "T" resistance network to model the electrical equivalent circuit of the intercalated disks. These simulations have demonstrated the minimal influence of the disk structures on the collision effects during repolarization when normal physiologic ranges in disk resistance were modeled.[4] Because of these previous studies, we felt justified in using a spatial step size that resulted in a reasonable amount of computer time necessary to simulate the transmural plane of the pulmonary conus. A much smaller spatial step increment would have changed the quantitative results by slightly reducing the computed conduction velocity and action potential duration changes. The two-dimensional model used in the simulations shown in Figure 6 was based on canine pulmonary conus fiber orientation previously reported.[8] Our tissue histology did not allow us to quantitatively assess the reported abrupt 90° fiber rotation, but it did confirm that fibers in the epicardial and endocardial portions of the pulmonary conus were orthogonally oriented. Incorporating gradual transmural fiber rotation in the model rather than abrupt transmural rotation would have altered coupling resistances but would not have qualitatively changed the activation patterns and epicardial APD distributions. Based on these considerations, the computer simulations are necessarily qualitative and do not prove the detailed mechanism of our experimental findings. However, we believe the proposed nonuniform anisotropy model does provide a reasonable explanation for the key features of our results. Thus, the model establishes a framework for further refinements as additional physiologic information is acquired.

The results of the present study have clinical implications. Although the focus of the study was to define the relation between epicardial activation delays and repolarization properties, electrotonic interactions at and near the delay sites also alter the action potential upstroke, producing changes in both the time course and time integral of the sodium current.[4] It is, therefore, possible that antiarrhythmic effects of agents that alter sodium current may be modulated to some extent by activation pattern and associated changes in sites of acceleration and deceleration of activation. In addition, it is possible that antiarrhythmic drugs that have different direct effects on longitudinal and transverse conduction velocity[39] may have indirect effects on repolarization properties. Another clinical implication is that an isochrone map during a single drive may not identify localized areas of high resistance parallel to propagation direction. As a corollary, it may be possible to infer the spatial distribution of zones of high cell-to-cell coupling resistance from isochrone maps of multiple activation orders. Certain disease states, such as myocardial infarction, are known to be associated with localized conduction defects, and the border zone between normal and ischemic myocardium is a region where a transition between normal and slow conduction is likely to occur.[27] Our findings indicate such regions could be susceptible to marked variations in the uniformity of both activation and repolarization properties when activation sequence is changed. Since conduction velocity and repolarization properties both play a role in vulnerability to ventricular arrhythmias, some ectopic sites could produce a more vulnerable state because they are associated with greater nonuniformity of activation and repolarization properties than other sites. Our findings imply that the site of origin of premature ectopic ventricular depolarizations could be an important factor in determining whether ectopic activity initiates ventricular tachyarrhythmias.

Appendix

The following is the theoretical basis for the NAI calculation and the effects of acceleration and deceleration on action potential configuration. The analytic derivation is similar to one previously reported for action potential collision,[5] but the goal here is different, namely, to define the electrotonic effects of a change in propagation velocity. During action potential propagation, two traveling waves of axial current move in the direction of propagation. The leading wave is due to action potential depolarization, and the trailing wave is due to action potential repolarization. In an infinitely long, homogeneous, one-dimensional cable, the charge

contained in the leading wave (Q_d, μC) is the negative of the charge contained in the trailing wave (Q_r, μC) and is determined by:

$$Q_r = \frac{APH\pi a^2}{R_i\theta} = -Q_d \quad (3)$$

where APH is the action potential height (mV), a is the cable radius (cm), R_i is the specific cell-to-cell resistivity (kΩcm), and θ is the conduction velocity (cm/sec).[5] Thus, the charge contained in axial current waves is determined by only action potential height, cable radius, cell-to-cell resistance, and conduction velocity.

The situation to be investigated is action potential propagation through the junction between two infinitely long one-dimensional cables positioned end-to-end. The difference in charge contained in the axial current waves between the two cables is the charge, defined by Equation 3, in the upstream cable minus the charge, defined by Equation 3, in the downstream cable. A charge imbalance, during both depolarization and repolarization, is the result of differences in any of the four parameters between the two cables. If the conduction velocity is the only difference between the two cables, the difference in charge in the axial current wave between the two cable halves (ΔQ_r, ΔQ_d, μC) is:

$$\Delta Q_r = \frac{APH\pi a^2}{R_i}\left(\frac{1}{\theta_A} - \frac{1}{\theta_B}\right) = -\Delta Q_d \quad (4)$$

where θ_A is the steady-state conduction velocity in the upstream cable (cm/sec), and θ_B is the steady-state conduction velocity in the downstream cable (cm/sec).

The charge differences, ΔQ_r and ΔQ_d, are dissipated (or supplied) at the cable junction and cause a change in transmembrane voltage at the cable junction, which spatially decays at a distance from the junction. The situation is similar to intracellular current injection at the junction. The voltage time area that accompanies transient current injection in an infinitely long cable is independent of the time course of the injected current,[40] and the area (A, mV/sec) at the junction due to the current injection is given by:

$$A = -Q\sqrt{R_m R_i/(\pi^2 8a^3)} \quad (5)$$

where Q is the total injected charge (μC), and R_m is the specific membrane resistance (kΩcm^2).[41] To be consistent with the frame of reference in this development, a positive Q has a hyperpolarizing effect on the membrane potential. Note that Equation 5 is equivalent to the charge multiplied by the input resistance of the cable.

The analysis is complicated by the fact that the charge is injected throughout the action potential when membrane resistance is time varying. However, as shown in our previous work,[5] the results are not significantly affected by assuming a membrane resistance during depolarization that is much smaller than a constant membrane resistance during repolarization (Rm_r, kΩcm^2). Thus, the effect of a change in conduction velocity on the change in action potential area at the junction (ΔAPA, mV/sec) can be determined using Equation 5 with the charge determined by Equation 4 and the membrane resistance defined as that during repolarization, neglecting the effect during depolarization. After substitution this becomes:

$$\Delta APA = -APH\sqrt{(aRm_r)/(8R_i)}\left(\frac{1}{\theta_A} - \frac{1}{\theta_B}\right) \quad (6)$$

In summary, nonuniform conduction (θ_A-θ_B) will cause electrotonic modulation of action potential configuration. Acceleration ($\theta_A<\theta_B$) will reduce action potential area, and deceleration ($\theta_A>\theta_B$) will increase action potential area.

The spatial change in conduction velocity can be written in differential notation as:

$$\frac{1}{\theta_A} - \frac{1}{\theta_B} = -\Delta x\left(\frac{d}{dx}\left(\frac{1}{\theta}\right)\right) \quad (7)$$

where Δx is the electrode spacing (cm). Since $\theta = dx/dt$:

$$\frac{1}{\theta_A} - \frac{1}{\theta_B} = -\Delta x\left(\frac{d}{dx}\left(\frac{dt}{dx}\right)\right) \quad (8)$$

$$\frac{1}{\theta_A} - \frac{1}{\theta_B} = -\Delta x\left(\frac{d^2t}{dx^2}\right) \quad (9)$$

Thus, ΔAPA is directly proportional to d^2t/dx^2, the second spatial derivative of time. The NAI used in the analysis of the animal experiments was a numerical estimate of Equation 9. Note that acceleration is the second temporal derivative of space (d^2x/dt^2), and NAI can be interpreted as spatial acceleration multiplied by the electrode spacing.

A diagram showing the theoretical results of the effect of spatial changes in conduction velocity on electrotonic current during repolarization is shown in Figure 7. For purposes of this presentation, a simplified three-cell cable was used to calculate the membrane current (I_m) of the middle cell during three conditions: 1) normal propagation with constant velocity, 2) deceleration, and 3) acceleration. The sequence of activation was the same in all cases: upstream cell, middle cell, and downstream cell. In this simplified model, the three action potential configurations were not based on Beeler-Reuter equations but were described by mathematical functions. All three action potential waveforms were identical, and since the cells were not allowed to interact, their action potential configurations were independent of I_m. The cells were not allowed to interact because with interaction, the change in action potential configuration would in turn change I_m, which would then further change action potential configuration and so on. In contrast, the noninteracting model was specifically chosen to simplify the situation by illustrating the maximum I_m current and maximum net charge during repolarization available to modulate action potential configuration if

the cells had been allowed to interact. The darkened area corresponds to ΔQ_r of Equation 4, which is the driving force in electrotonically modulating action potential area. This model differs from an interactive Beeler-Reuter model in that the I_m in the latter case is attenuated somewhat by the source and input impedances of the interacting cells. In the upper panel, the cells were assigned activation times that resulted in uniform conduction velocity, and the net I_m during repolarization (darkened area) was zero. In the middle panel, the cells were assigned activation times that resulted in deceleration at the middle cell. At this deceleration site, the net I_m during repolarization was positive, and action potential duration of this cell would have prolonged if the cells had been allowed to interact. The cells in the bottom panel were assigned activation times that resulted in acceleration. Under these conditions, the net I_m during repolarization was negative, and action potential duration of this cell would have shortened if the cells had been allowed to interact.

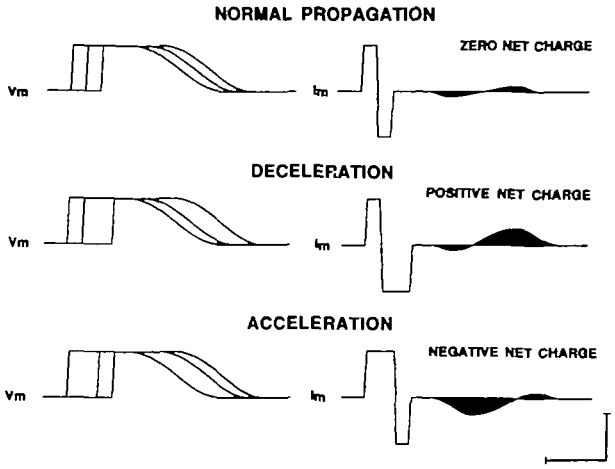

FIGURE 7. *Effect of propagation with uniform conduction velocity* (upper panel), *deceleration* (middle panel), *and acceleration* (lower panel) *on membrane current in a noninteracting three-cell cable. This figure illustrates theoretic results derived in "Appendix." Vm represents cellular transmembrane potentials. All three action potentials have identical configurations.* Left panel *shows temporal relation of the three action potentials that occurred with excitation initiated at the upstream cell.* Right panel *shows resulting membrane current (I_m) that would be available to electrotonically modulate center cell as activation proceeds from upstream cell to middle cell and then to downstream cell if cells were allowed to interact. Shaded areas correspond to net I_m current during repolarization. A positive area would depolarize the cell and prolong action potential duration, while a negative area would hyperpolarize the cell and shorten action potential duration. Normal propagation with constant conduction velocity resulted in zero net charge during repolarization. Deceleration caused a positive net charge during repolarization while acceleration caused a negative net charge during repolarization. All cells were coupled with 1 kΩ resistors. Calibration bars are 100 mV (Vm), 100 μA (I_m), and 100 msec (Vm and I_m).*

Acknowledgments

We greatly appreciate Dr. Elizabeth Hammond's expert assistance in preparation and evaluation of the histologic specimens in this study. We also thank Ms. Leona Archuleta for her excellent secretarial assistance and Ms. Jayne Davis for help in preparing the figures.

References

1. Abildskov JA: Effects of activation sequence on local recovery of ventricular excitability in the dog. *Circ Res* 1976;38: 240–243
2. Toyoshima H, Burgess MJ: Electrotonic interaction during canine ventricular repolarization. *Circ Res* 1978;43:348–356
3. Burgess MJ, Steinhaus BM, Spitzer KW, Green LS: Effects of activation sequence on ventricular refractory periods of ischemic canine myocardium. *J Electrocardiol* 1985;18:323–330
4. Steinhaus BM, Spitzer KW: Simulation of activation sequence effects in heart tissue. *Proc IEEE/Frontiers of Engineering and Computing in Health Care Conference*, Columbus, Ohio, Sept 1983, pp 199–204
5. Steinhaus BM, Spitzer KW, Isomura S: Action potential collision in heart tissue. Computer simulations and tissue experiments. *IEEE Trans Biomed Eng BME* 1985;32:731–742
6. Steinhaus BM, Spitzer KW, Burgess MJ: Conduction delays as revealed by activation pattern (abstract). *Proc Banff Satellite Symposium on Cardiac Muscle Conf*, 1986 (in press)
7. Burgess MJ, Steinhaus BM, Spitzer KW, Ershler PR: Role of nonuniform activation on repolarization (abstract). *Circulation* 1986;74(suppl II):II–351
8. Armour JA, Randall WC: Structural basis for cardiac function. *Am J Physiol* 1970;218:1517–1523
9. Ershler PR, Steadman BW, Wyatt RF, Lux RL, Abildskov JA: A 64 lead online system for clinical and experimental mapping of ventricular activation sequences. *Proc Computers in Cardiology*, Park City, Utah, Sept, 1984, pp 417–419
10. Ershler PR, Lux RL, Steadman BW: A 129 lead online intraoperative mapping system. Invited paper for *IEEE Engineering in Medicine and Biology Society's 8th Annual Conference*, Ft Worth, Tex, November 7-10, 1986, pp 1289–1291
11. Joyner RW, Overholt ED, Ramza B, Veenstra RD: Propagation through electrically coupled cells: Two inhomogeneously coupled cardiac tissue layers. *Am J Physiol* 1984;247: H596–H609
12. Beeler GW, Reuter H: Reconstruction of the action potential of myocardial fibres. *J Physiol* (Lond) 1977;268:177–210
13. Spach MS, Dolber PC: The relation between discontinuous propagation in anisotropic cardiac muscle and the "vulnerable period" of reentry, in Zipes DC, Jalife J (eds): *Cardiac Electrophysiology and Arrhythmias*, Orlando, Fla, Grune and Stratton, 1985, pp 241–252
14. Roberge FA, Vinet A, Victorri B: Reconstruction of propagated electrical activity with a two-dimensional model of anisotropic heart muscle. *Circ Res* 1986;58:461–475
15. Spach MS, Dobler PC, Kootsey JM, Johnson EA: Accounting for anisotropic behavior of propagation by directional differences of membrane capacity in human cardiac cells (abstract). *Circulation* 1986;74(suppl II):II-419
16. Crank J, Nicholson P: A practical method for numerical evaluation of solutions of partial differential equations of the heat-conduction type. *Proc Camb Philos Soc (Math Phys Sci)* 1947;43:50–67
17. Peaceman DW, Rachford HH: Numerical solution of parabolic and elliptic differential equations. *J Soc Indust Appl Math* 1965;3:28–41
18. von Rosenberg DU: Alternating-direction-implicit methods. *Methods for the Numerical Solution of Partial Differential Equations*. New York, American Elsevier Publishing Co, 1969, pp 87–89
19. Joyner RW, Ramon F, Moore JW: Simulation of action potential propagation in an inhomogeneous sheet of coupled excitable cells. *Circ Res* 1975;36:654–661
20. Steinhaus BM, Spitzer KW, Burgess MJ, Abildskov JA: Electrotonic interactions in a model of anisotropic cardiac

tissue. *Proc 1986 Summer Computer Simulation Conf*, 1986, 421–426
21. Plonsey R: *Bioelectric Phenomena*. New York, McGraw-Hill, 1969, pp 202–275
22. Spach MS, Miller WT III, Miller-Jones E, Warren RB, Barr RC: Extracellular potentials related to intracellular action potential during impulse conduction in anisotropic canine muscle. *Circ Res* 1979;45:188–204
23. Draper MH, Mya-Tu M: A comparison of the conduction velocity in cardiac tissues of various mammals. *J Exp Physiol* 1959;44:91–109
24. Clerc L: Directional differences of impulse spread in trabecular muscle from mammalian heart. *J Physiol* 1976;255:335–346
25. Roberts DE, Hersh LT, Scher AM: Influence of cardiac fiber orientation on wavefront voltage, conduction velocity and tissue resistivity in the dog. *Circ Res* 1979;44:701–712
26. Spach MS, Miller WT, Geselowitz DB, Barr RC, Kootsey JM, Johnson EA: The discontinuous nature of propagation in normal canine cardiac muscle. Evidence for recurrent discontinuities of intracellular resistance that affect the membrane currents. *Circ Res* 1981;48:39–54
27. Kleber AG, Janse MJ, Wilms-Schopmann IG, Wilde AAM, Coronel R: Changes in conduction velocity during acute ischemia in ventricular myocardium of the isolated porcine heart. *Circulation* 1986;73:189–198
28. Tsuboi N, Kodama I, Toyama J, Yamada K: Anisotropic conduction properties of canine ventricular muscles – Influence of high extracellular K+ concentration and stimulation frequency. *Jpn Circ J* 1985;49:487–498
29. Spach MS, Miller WT, Dolber PC, Kootsey JM, Sommer JR, Mosher CE: The functional role of structural complexities in the propagation of depolarization in the atrium of the dog. Cardiac conduction disturbances due to discontinuities of effective axial resistivity. *Circ Res* 1982;50:175–191
30. Spach MS, Dolber PC: Relating extracellular potentials and their derivatives to anisotropic propagation at a microscopic level in human cardiac muscle. Evidence for electrical uncoupling of side-to-side fiber connections with increasing age. *Circ Res* 1986;58:356–371
31. Spach MS, Barr RC, Serwer GS, Johnson EA, Kootsey TM: Collision of excitation waves in the dog Purkinje system. *Circ Res* 1971;29:499–511
32. Ushiyama J: Cardiac action potentials recorded from the site at which two impulses of excitation have collided, in Kao FF, Koizumi K, Vassalle M (eds): *Research in Physiology*. Bologna, Italy, A Lieber Memorialis, Aulo Gagg, 1971, pp 37–43
33. Paes de Carvalho A, Saldena TA, Garcia EAC, Campos de Carvalho AC, Tashiro T, Paula Carvalho M: Homogeneous and nonhomogeneous conduction of impulses in heart and other excitable tissues, in Paes de Carvalho A, Hoffman BF, Lieberman M (eds): *Normal and Abnormal Conduction in the Heart*. Mount Kisco, New York, Futura, 1982, pp 117–143
34. Kootsey JM, Johnson EA: The origin of the T-wave. *CRC Crit Rev Bioeng* 1980;4:233–270
35. Tasaki I: Collision of two nerve impulses in the nerve fiber. *Biochim Biophys Acta* 1949;3:494–497
36. Goldstein SS, Rall W: Changes of action potential shape and velocity for changing core conductor geometry. *Biophys J* 1974;14:731–757
37. Joyner RW, Veenstra R, Rawling D, Chorro A: Propagation through electrically coupled cells. Effect of a resistive barrier. *Biophys J* 1984;45:1017–1025
38. Joyner RJ: Effects of the discrete pattern of electrical coupling on propagation through on electrical syncytrum. *Circ Res* 1982;50:192–200
39. Kadish AH, Spear JT, Levine JH, Moore EN: The effects of procainamide on conduction in anisotropic canine ventricular myocardium. *Circulation* 1986;74:616–625
40. Jack JJB, Noble D, Tsien RW: *Electric Current Flow in Excitable Cells*. Oxford, England, Clarendon, 1983, pp 187–188
41. Jack JJB: An introduction to linear cable theory, in Schmitt FOR, Worden FG (eds): *The Neurosciences Fourth Study Program*. Cambridge, Mass, MIT Press, 1979, pp 426–437

KEY WORDS • nonuniform activation • refractory periods • electrotonus • computer simulations • activation sequence • anisotropy

Circulation Research
JOURNAL OF THE AMERICAN HEART ASSOCIATION

Nonuniform epicardial activation and repolarization properties of in vivo canine pulmonary conus.

M J Burgess, B M Steinhaus, K W Spitzer and P R Ershler

Circ Res. 1988;62:233-246
doi: 10.1161/01.RES.62.2.233
Circulation Research is published by the American Heart Association, 7272 Greenville Avenue, Dallas, TX 75231

Print ISSN: 0009-7330. Online ISSN: 1524-4571